



Biomedical Engineering

Magnetic Resonance Spectroscopy 4 (MRS)

Dr. Stefan Kirsch



Computer Assisted Clinical Medicine
Faculty of Medicine Mannheim
University of Heidelberg
Theodor-Kutzer-Ufer 1-3
D-68167 Mannheim, Germany
Stefan.Kirsch@MedMa.Uni-Heidelberg.de
www.ma.uni-heidelberg.de/inst/cbtlm/ckm/



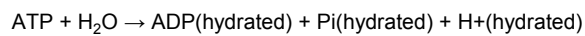
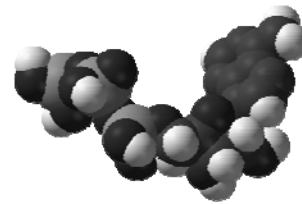
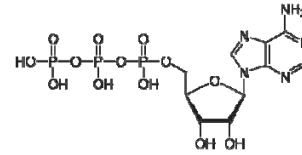
nucleus	spin I	gyromagnetic ratio γ [$10^8 \text{ rad s}^{-1} \text{ T}^{-1}$]	natural abundance of isotope in %	sensitivity ξ for $B_0 = \text{const.}$ in % (rel. to ^1H)
^1H	1/2	2,675	99,98	100,00
^{19}F	1/2	2,518	100,00	83,40
^{23}Na	3/2	0,708	100,00	9,27
^{31}P	1/2	1,084	100,00	6,65
^2H	1	0,410	0,01	$9,60 \times 10^{-1}$
^{12}C	0	-	98,89	-
^{13}C	1/2	0,673	1,11	$1,75 \times 10^{-2}$
^{14}N	1	0,193	99,63	$1,00 \times 10^{-1}$
^{16}O	0	-	99,76	-
^{17}O	5/2	-0,363	0,04	$1,11 \times 10^{-3}$
^{35}Cl	3/2	0,262	75,77	$3,58 \times 10^{-1}$
^{39}K	3/2	0,125	93,26	$4,76 \times 10^{-2}$
^{25}Mg	5/2	-0,164	10,00	$2,68 \times 10^{-2}$
^{43}Ca	7/2	-0,180	0,14	$8,68 \times 10^{-4}$
^{33}S	3/2	0,205	0,75	$1,70 \times 10^{-3}$

Phosphorus-31 (³¹P) Spectroscopy II

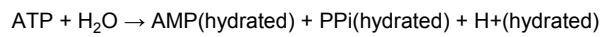


ATP (Adenosine triphosphate)

- ATP is the main energy source for the majority of cellular functions.
- This includes the synthesis of macromolecules, including DNA, RNA, and proteins.
- Energy released by cleaving either a phosphate (Pi) or pyrophosphate (PPi) unit from ATP:



$$\Delta G^\circ = -30.54 \text{ kJ/mol } (-7.3 \text{ kcal/mol})$$



$$\Delta G^\circ = -45.6 \text{ kJ/mol } (-10.9 \text{ kcal/mol})$$

ADP = Adenosindiphosphate, AMP = Adenosinmonophosphat

Phosphorus-31 (³¹P) Spectroscopy III



A: ³¹P spectra from rat skeletal muscle

B: ³¹P spectra from rat brain

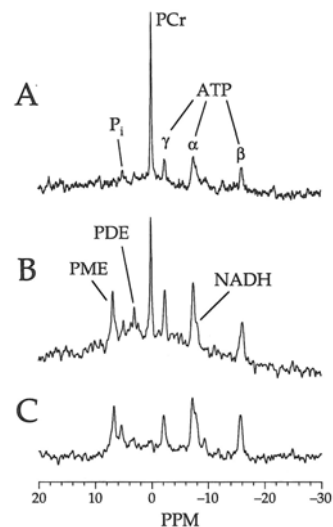
C: ³¹P spectra from rat liver

P_i = phosphate

PME = phosphomonoester

PDE = phosphodiester

NADH = Nicotinamide adenine dinucleotide



R. A. de Graaf, *In vivo* NMR Spectroscopy,
Principles and techniques

Fluorine-19 (¹⁹F) Imaging I



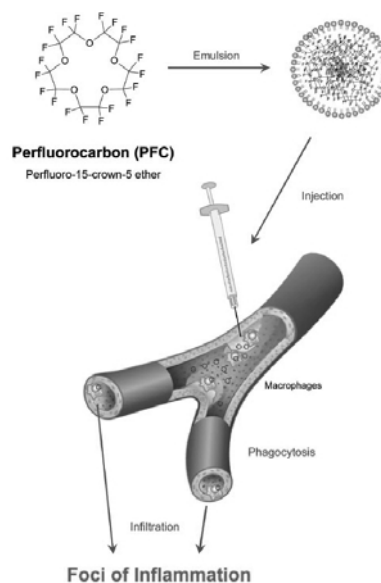
nucleus	spin /	gyromagnetic ratio γ [10 ⁸ rad s ⁻¹ T ⁻¹]	natural abundance of isotope in %	sensitivity ξ for B ₀ = const. in % (rel. to ¹ H)
¹ H	1/2	2,675	99,98	100,00
¹⁹ F	1/2	2,518	100,00	83,40
²³ Na	3/2	0,708	100,00	9,27
³¹ P	1/2	1,084	100,00	6,65
² H	1	0,410	0,01	9,60 × 10 ⁻¹
¹² C	0	-	98,89	-
¹³ C	1/2	0,673	1,11	1,75 × 10 ⁻²
¹⁴ N	1	0,193	99,63	1,00 × 10 ⁻¹
¹⁶ O	0	-	99,76	-
¹⁷ O	5/2	-0,363	0,04	1,11 × 10 ⁻³
³⁵ Cl	3/2	0,262	75,77	3,58 × 10 ⁻¹
³⁹ K	3/2	0,125	93,26	4,76 × 10 ⁻²
²⁵ Mg	5/2	-0,164	10,00	2,68 × 10 ⁻²
⁴³ Ca	7/2	-0,180	0,14	8,68 × 10 ⁻⁴
³³ S	3/2	0,205	0,75	1,70 × 10 ⁻³

Fluorine-19 (¹⁹F) Imaging II



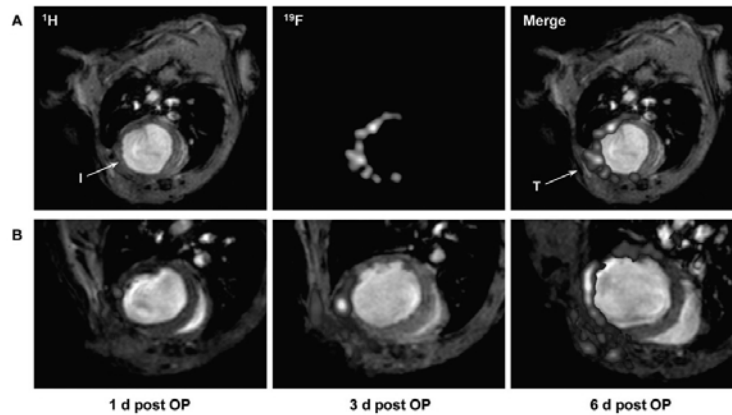
Perfluorocarbons (PFCs) for monitoring of inflammatory processes

- Injection, emulsified particles are taken up by the monocyte/macrophage system and transported to areas of inflammation.
- Because of the lack of any ¹⁹F background signal, the detected signals are highly specific for infiltrating immunocompetent cells loaded with PFCs.



U. Fögel *et al.*,
Circulation 8, 140-148
(2008)

Fluorine-19 (^{19}F) Imaging III



U. Fögel *et al.*,
Circulation 8, 140-148
(2008)

Infiltration of PFCs after myocardial infarction as detected by in vivo ^{19}F MRI.

A: Anatomically corresponding ^1H and ^{19}F images from the mouse thorax recorded 4 days shows accumulation of ^{19}F signal near the infarcted region (I). PFCs were injected at day 0 via the tail vein.

B: Sections of ^1H images superimposed with the matching ^{19}F images (red) acquired 1, 3, and 6 days after surgery (T).

Fluorine-19 (^{19}F) Imaging IV

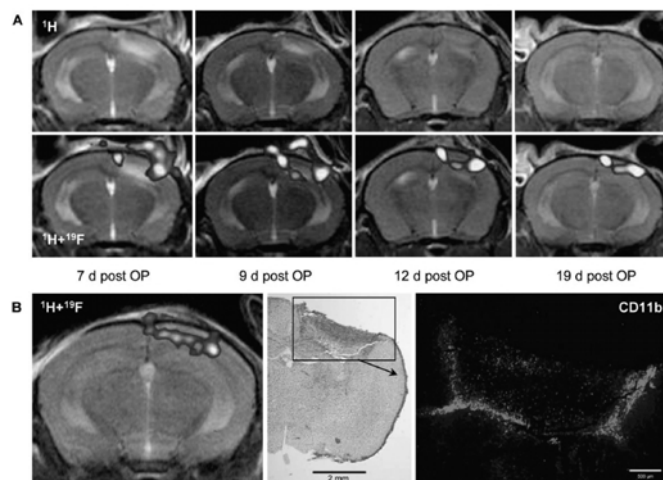


Infiltration of PFCs into the brain after induction of focal cerebral ischemia.

A: movement of the PFCs with the rim of the infarct over time.

B: In vivo and postmortem brain images acquired 7 days after induction of focal cerebral ischemia.

Left, Section of merged ^1H and ^{19}F images taken immediately before organ excision. Middle, Microscopic survey of the injured hemisphere. The black rectangle represents the section displayed in the adjoining fluorescence image.



U. Fögel *et al.*, *Circulation* 8, 140-148 (2008)

Sodium-23 (^{23}Na) Spectroscopy & Imaging I



nucleus	spin I	gyromagnetic ratio γ [$10^8 \text{ rad s}^{-1} \text{ T}^{-1}$]	natural abundance of isotope in %	sensitivity ξ for $B_0 = \text{const.}$ in % (rel. to ^1H)
^1H	1/2	2,675	99,98	100,00
^{19}F	1/2	2,518	100,00	83,40
^{23}Na	3/2	0,708	100,00	9,27
^{31}P	1/2	1,084	100,00	6,65
^2H	1	0,410	0,01	$9,60 \times 10^{-1}$
^{12}C	0	-	98,89	-
^{13}C	1/2	0,673	1,11	$1,75 \times 10^{-2}$
^{14}N	1	0,193	99,63	$1,00 \times 10^{-1}$
^{16}O	0	-	99,76	-
^{17}O	5/2	-0,363	0,04	$1,11 \times 10^{-3}$
^{35}Cl	3/2	0,262	75,77	$3,58 \times 10^{-1}$
^{39}K	3/2	0,125	93,26	$4,76 \times 10^{-2}$
^{25}Mg	5/2	-0,164	10,00	$2,68 \times 10^{-2}$
^{43}Ca	7/2	-0,180	0,14	$8,68 \times 10^{-4}$
^{33}S	3/2	0,205	0,75	$1,70 \times 10^{-3}$

Sodium-23 (^{23}Na) Spectroscopy & Imaging II



Sodium \rightarrow spin 3/2 nuclei (nucleus has a electrical quadrupol moment)

Energy levels are given by:

$$E_m = -\gamma \hbar m B_0 \quad ; \quad m = -I, I+1, \dots, I$$

$\Rightarrow I = 3/2 \Rightarrow 4$ equidistant energy levels

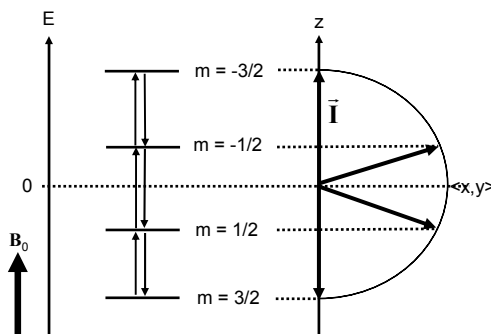
\Rightarrow two possible transitions (inner $\uparrow\downarrow$ and outer $\uparrow\downarrow$ transitions)

\Rightarrow generally two relaxation paths (two relaxation rates)

$$M_z \propto M_0 \left[a \exp(-t/T_{1,a}) + b \exp(-t/T_{1,b}) \right]$$

$$M_{xy} \propto M_0 \left[a \exp(-t/T_{2,a}^*) + b \exp(-t/T_{2,b}^*) \right]$$

$a, b \rightarrow$ inner, outer transition



Sodium-23 (^{23}Na) Spectroscopy

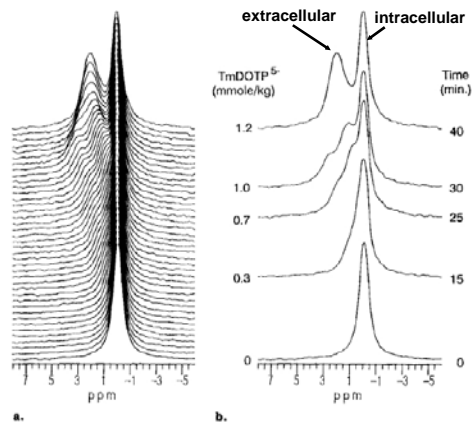


Observation of intra- and extracellular ^{23}Na using chemical shift agents

Chemical shift agent accumulates extracellular!

Na-^{23} MR spectra of rat brain during infusion of the shift reagent Tm-DOTP $^{5-}$

- (a) Stacked plot of 40 spectra collected over 40 minutes in a representative animal
- (b) spectra collected initially ($t = 0$) and after 15, 25, 30, and 40 minutes of shift reagent infusion are shown



N. Bansal et al., JMIRI
2, 385-391 (1992)

Hyperpolarization I



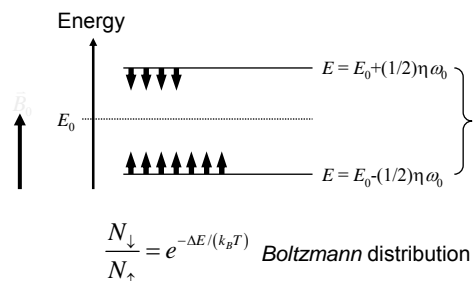
How can we "boost" the signal?

- remember spin-1/2 system in external field B_0 :

- Def. Polarization P :
$$P \equiv \frac{N_{\uparrow} - N_{\downarrow}}{N_{\uparrow} + N_{\downarrow}}$$

- **Signal** $\propto P$:

- P can be evaluated as
$$P = \tanh\left(\frac{\gamma \hbar B_0}{2k_B T}\right)$$



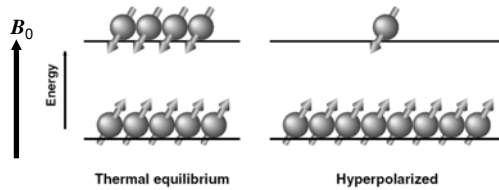
Hyperpolarization II



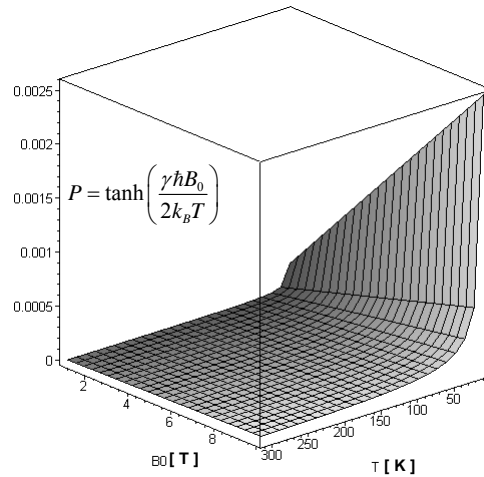
The “brute force” approach

⇒ temperature down, external field up

Nucleus	Polarization P_1 at 1.5 T, 310 K	Polarization P_2 at 20 T, 4 K	Ratio P_2/P_1
^1H	$4.9 \cdot 10^{-6}$	$5.1 \cdot 10^{-3}$	1033
^3He	$3.8 \cdot 10^{-6}$	$3.9 \cdot 10^{-3}$	1033
^{13}C	$1.2 \cdot 10^{-6}$	$1.3 \cdot 10^{-3}$	1033
^{129}Xe	$1.4 \cdot 10^{-6}$	$1.4 \cdot 10^{-3}$	1033



- available signal will depend on concentration of the imaging agent ⇒ only a small amount can be administered (10^{-3} to 10^{-6} of natural ^1H conc. in human body!) ⇒ polarization increase of ~1000 is not sufficient



Hyperpolarization III



The breakthrough: optical pumping

- In 1958, Franken and Colegrove showed that hyperpolarization can be achieved by optical pumping and metastability exchange.
- In 1960, Bouchiat *et al.* showed: angular momentum of optically pumped e^- spins of Rb atoms could be transferred to nuclear spins of ^3He by spin-exchange collision
- Method (Bouchiat) also works for ^{129}Xe

Principle:

1. generate a highly polarized electron system
2. transfer of the polarization to the nuclear spin system

Hyperpolarization IV



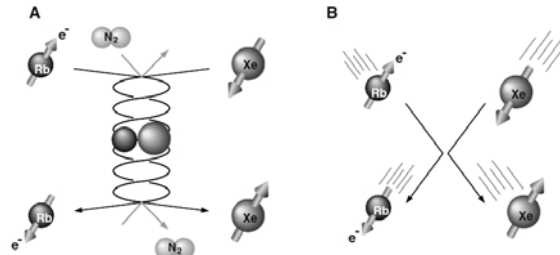
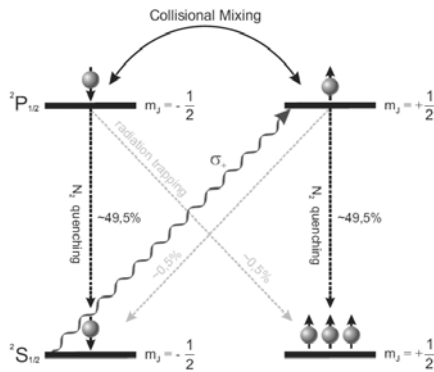
Hyperpolarization by spin-exchange collisions

Generate polarized e-system

- e^- of rubidium ^{37}Rb is excited in $m=+1/2$ state (high energy)
- continuous excitation populates (polarizes) $m=+1/2$ state (low energy)

Transfer polarization to nuclear spin system

- via loosely bound van der Waals molecules
- via binary collisions



Hyperpolarization V



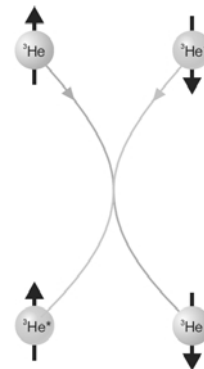
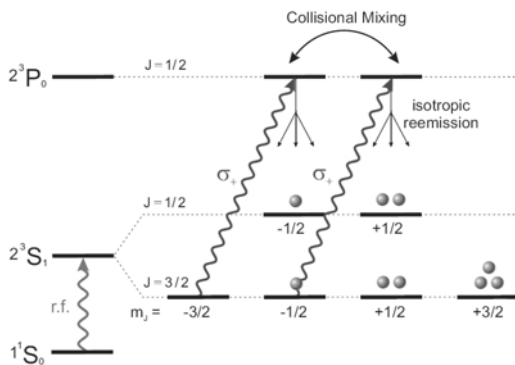
Hyperpolarization by metastability exchange

Generate polarized e-system

- electronic state of ^3He is excited in the 2^3S_1 state via rf irradiation or electric discharge
- continuous excitation populates a metastable electronic state

Transfer polarization to nuclear spin system

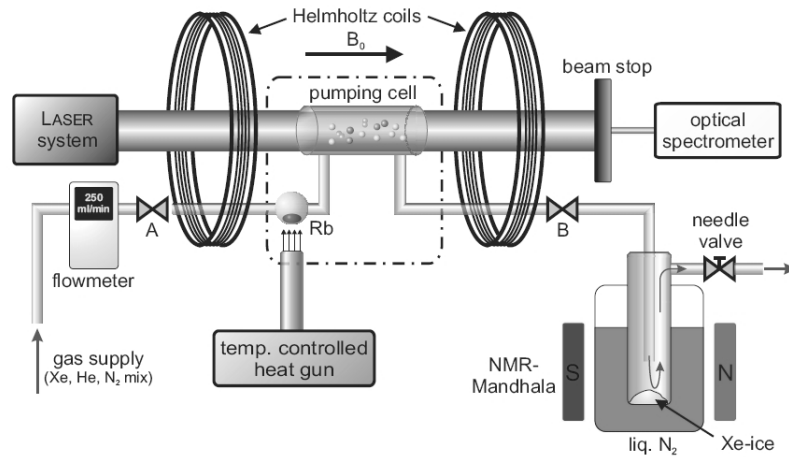
- via metastability exchange collisions



Hyperpolarization VI

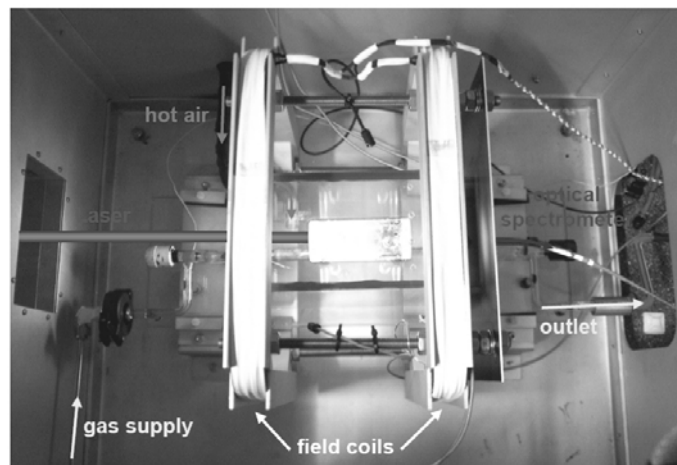


Experimental setup for hyperpolarization of ^{129}Xe by spin-exchange collisions



P.-P. Zänker, PhD Thesis, Mainz 2007

Hyperpolarization VII



P.-P. Zänker, PhD Thesis,
Mainz 2007

^{129}Xe polarizer during the polarization process. The picture was taken with an infrared-sensitive camera, so that the usually invisible fluorescence light of the rubidium excitation is depicted clearly.

Hyperpolarization VIII



P-P. Zänker, PhD Thesis,
Mainz 2007

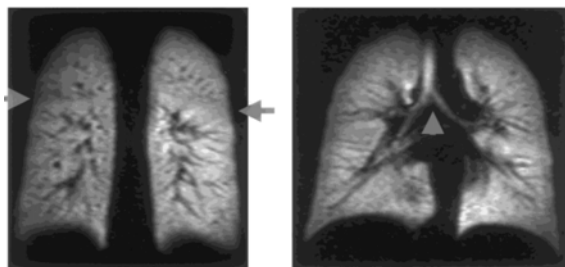
^3He polarizer at the Institut für Physik at the university of Mainz. The optical system, guiding the laser light, is depicted at the left side. The blue fluorescence light in the pumping cells due to the electric discharge can be seen on the right hand side.

Hyperpolarization IX

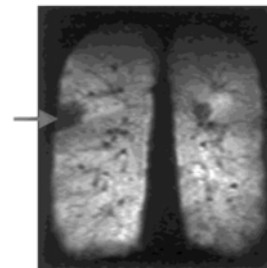


^3He MRI of the human lung

Coronal ^3He images of a healthy
volunteer



Coronal ^3He images of a
asthmatic with ventilation defect
(arrow)



T.A. Altes,
JMIRI 13, 378-384 (2001)

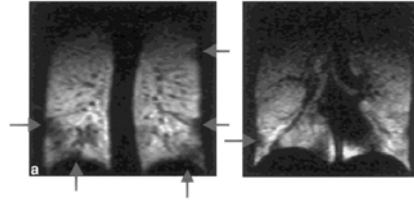
Hyperpolarization X



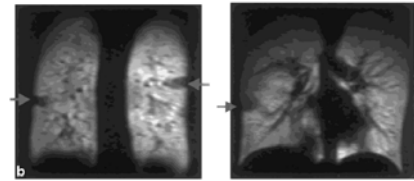
^3He MRI of the human lung

T.A. Altes *et al.*,
JMIRI 13, 378-384 (2001)

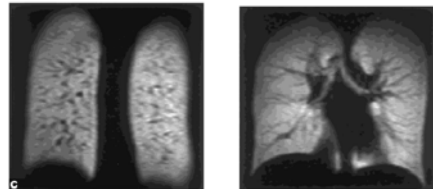
a: Mildly symptomatic asthmatic.
Multiple ventilation defects
(arrows) are present
throughout the lungs.



b: Images of the same
individual, obtained three weeks
later and at the same anatomic
levels as in Figure a, show that
the multiple ventilation defects
(arrows) are in different locations.



c: Images at the same levels, obtained 30 minutes after Figure
b, show that the ventilation defects resolved completely
following the use of an inhaled bronchodilator.



Hyperpolarization XI

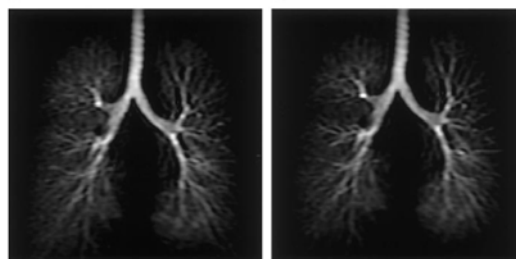
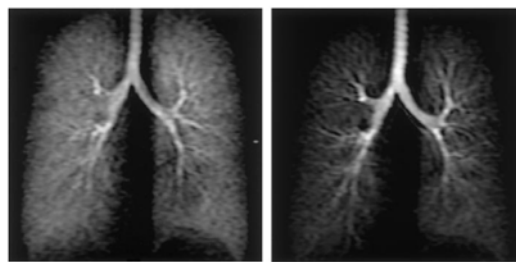


^3He MRI of the human lung

Time series of dynamic coronal projection images of the
lung acquired during inhalation of hyperpolarized ^3He .

As the inhalation continued, the SNR in the airways
increased while the SNR in the lung periphery remained
constant.

On images obtained during **(a, b)** early inhalation, the
distal airways are not as clearly distinguishable from the
lung periphery as on images obtained during **(c, d)** late
inhalation.



A. C. Tooker *et al.*,
Radiology Vol 227, Nr 2,
575-579 (2003)

Hyperpolarization XII



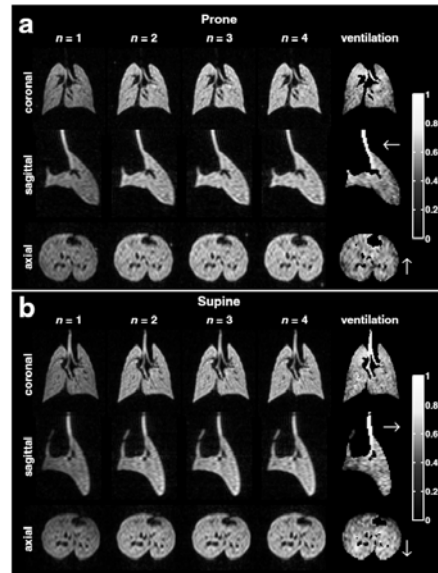
^3He MRI of the rat lung

Coronal, sagittal and axial slices from 3D acquisitions after n helium breaths in **prone** (a) and **supine** (b) postures (rat).

The rightmost column shows the regional ventilation map calculated from the four columns on the left. The arrows indicate the dependent direction.

In supine position, higher ventilation in the dependent parts can be seen in the sagittal and axial **ventilation maps**.

Prone = lying on the breast (a)
Supine = lying on the back (b)

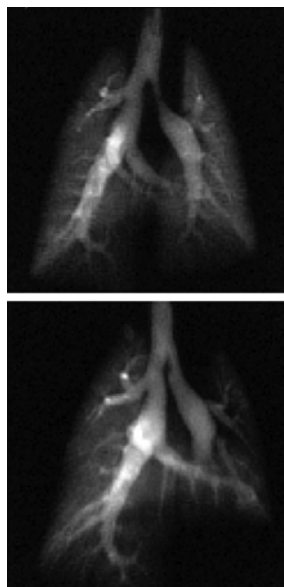


S. Månsson et al., J. Appl. Physiol. 98, 2259-2267 (2005)

Hyperpolarization XIII



^{129}Xe MRI of the rat lung



B. Driehuys et al., PNAS, Vol 103, Nr 48, 18276-18283

Summary Lecture MRS 1



- **Origin of nuclear magnetism:** - magnetic moment of the nucleus
- intrinsic magnetic moment of the electron
- currents from unpaired orbital electrons
- **Energy of a magnetic moment in an external magn. field:** $E = -\vec{\mu} \cdot \vec{B}$
- **External static field** \Rightarrow precession of the magnetization
- **Bloch equations** (with and without relaxation)
- **Relaxation in liquids:** - transitions between *Zeeman* energy levels in order to reestablish the *Boltzmann* distribution \Rightarrow longitudinal relaxation

- irreversible dephasing \Rightarrow transversal relaxation
- caused by molecular tumbling motion \Rightarrow correlation time
- resonance phenomenon \Rightarrow spectral density function
- **Measurement of relaxation times**

- spin echo $\Rightarrow T_2$
- inversion recovery $\Rightarrow T_1$

Summary Lecture MRS 2



- **The NMR hardware:** magnet, gradient system (localization), receive & transmit coils, complex receiver signal, Nyquist-Shannon sampling theorem
- **The FID Experiment:** multiple (N) transients $\Rightarrow s/n \propto (N)^{1/2}$
- **Fourier transform:** complex exponential decay \Rightarrow complex Lorentzian, spectral phase shifts
- **Chemical shift:** induced fields via molecular electronic currents, shielding & deshielding the external field
- **J -coupling:** coupling of nuclear spins via bonding electrons \Rightarrow multiplet structure spectra
- **2D spectroscopy:** the COSY experiment, two time domains \Rightarrow 2D Fourier transform \Rightarrow 2D freq. domain, analysis of complex spectra (e.g. proteins)

Summary Lecture MRS 3



- **Localization in MRS:** - single voxel → 3 orthogonal slices (STEAM / PRESS)
 - multi voxel → 2D phase encoding
- **J-modulation:** - multiplets are modulated with $\cos(\pi \cdot TE \cdot J)$ → spectral editing
- **water suppression:** - signal H_2O / signal metabolites $\sim 10^4$
- **Important brain metabolites:** NAA, Cho, Cr, PCr, Lac, Glu, Gln, ml, Glc, GABA
- **other important metabolite:** citrate (Ci, prostate cancer)
- **Increasing B_0 :** → higher spectral resolution, higher s/n (but also more technical problems)

Summary Lecture MRS 4



- **Phosphorus 31 (^{31}P) MRS:** access to important metabolites (ATP)
- **Flourine 19 (^{19}F) MRI:** perflourcarbons (PFCs) as cellular marker
- **Sodium (^{23}Na) MRS & MRI:** ⇒ ^{23}Na → spin 3/2 → electric quadrupol moment
 - ⇒ 4 equidistant energy levels
 - ⇒ generally two relaxation rates $1/T_1$ and $1/T_2$ ($1/T_2^*$)
 - ⇒ access to sodium-potassium pump
 - ⇒ discrimination between intra- and extracellular sodium via chemical shift agents
- **Hyperpolarization:** ⇒ Principle:
 1. generate highly polarized e^- system
 2. transfer e^- polarization to nuclear spin system⇒ Application: Lung imaging